

# Light-Induced Subpicosecond Topological Phase Transition by Tuning Magnetic Order in Antiferromagnetic Dirac Semimetal EuAgAs

Hao Liu,<sup>1</sup> Chen Zhang,<sup>1</sup> Qi-Yi Wu,<sup>1</sup> Yahui Jin,<sup>2</sup> Ziming Zhu,<sup>2</sup> Jiao-Jiao Song,<sup>1</sup> Honghong Wang,<sup>3</sup> Bo Chen,<sup>1</sup> Jun He,<sup>1</sup> Hai-Yun Liu,<sup>4</sup> Yu-Xia Duan,<sup>1</sup> Peter M. Oppeneer,<sup>5,\*</sup> and Jian-Qiao Meng<sup>1,†</sup>

<sup>1</sup>*School of Physics, Central South University, Changsha, Hunan 410083, China*

<sup>2</sup>*Key Laboratory of Low-Dimensional Quantum Structures and Quantum Control of Ministry of Education, Department of Physics, Hunan Normal University, Changsha, Hunan 410081, China*

<sup>3</sup>*Center for Quantum Materials and Superconductivity (CQMS) and*

*Department of Physics, Sungkyunkwan University, Suwon 16419, South Korea*

<sup>4</sup>*Beijing Academy of Quantum Information Sciences, Beijing 100085, China*

<sup>5</sup>*Department of Physics and Astronomy, Uppsala University, Box 516, S-75120 Uppsala, Sweden*

(Dated: November 19, 2024)

We report the observation of a light-induced subpicosecond topological phase transition in the antiferromagnetic Dirac semimetal EuAgAs, achieved through precise manipulation of its magnetic configuration. Using ultrafast optical spectroscopy, we probe the nonequilibrium carrier dynamics and reveal a magnetic-order-driven transition between distinct topological states. Our results demonstrate that EuAgAs, with its highly tunable magnetic structure, offers a unique platform for exploring topological phase transitions, distinct from conventional methods like Floquet engineering, coherent-phonon excitation, and lattice structural modifications. These results underscore the potential of ultrashort optical pulses as powerful tools for real-time control of topological phases, opening pathways for advances in spintronics, quantum computing, and energy-efficient information technologies.

Magnetic topological materials are of considerable interest due to the coupling between magnetism and topological states, which can lead to the emergence of exotic quantum phenomena such as the quantum anomalous Hall effect [1, 2], topological magnetoelectric effects [3, 4], and the topological Hall effect [5–7]. A defining characteristic of these materials is the ability to drive topological phase transitions through the control of magnetic ordering [6–13]. This capability holds promise for developing new spintronics, quantum computing architectures, and energy-efficient information storage technologies.

Eu-based rare-earth compounds, known for their strong spin-orbit coupling and magnetic interactions mediated by localized  $4f$  electrons, have gained attention as promising candidates for realizing tunable magnetic topological states. Materials like  $\text{EuIn}_2\text{As}_2$  [14, 15] and  $\text{EuCd}_2\text{As}_2$  [16, 17] exhibit magnetic topological phases that respond sensitively to external perturbations such as magnetic fields and strain, enabling transitions between Dirac and Weyl semimetal states. This makes them ideal platforms for exploring the rich interplay between magnetism and topology.

In this context, EuAgAs, an antiferromagnetic (AFM) Dirac semimetal with a Néel temperature ( $T_N$ ) of 12 K, has recently been identified as a promising candidate for further investigation [18–20]. The material’s  $A$ -type AFM order, with ferromagnetic (FM) coupling within Eu hexagonal layers and AFM coupling between layers along the  $c$ -axis [20, 21], drives several interesting topological transitions. Previous studies have reported the observation of chiral anomaly-induced positive longitudinal magnetoconductivity in materials, which

has been interpreted as evidence for the generation of Weyl fermion states under the influence of an applied magnetic field [20]. Despite these advances, direct experimental observation of the evolution of topological band structure in response to changes in magnetic order remains an elusive goal.

Ultrafast laser spectroscopy offers a powerful tool for probing and manipulating topological materials [22, 23]. By rapidly perturbing the energy landscape, this technique allows for the detection of subtle changes in electronic structure and the induction of topological phase transitions. Previous studies have demonstrated the efficacy of ultrafast spectroscopy in investigating high-temperature superconductors [24–26], heavy fermion systems [27, 28], and topological materials [29–32]. However, unlike conventional ultrafast spectroscopy methods used to induce topological phase transitions, such as Floquet engineering [[33–35], coherent-phonon excitation [31], or lattice structure modification [32, 36], our approach here focuses on achieving topological transitions by tuning the magnetic configuration of EuAgAs. The metamagnetic nature of EuAgAs [20], coupled with the proximity of its Fermi level to Dirac points in all topological states [18, 20], makes it highly susceptible to external perturbations [18–20], including magnetic fields, strain, and pressure. These unique characteristics provide a direct and distinct route to controlling topological phase transitions, offering new insights beyond traditional topological manipulation techniques.

In this letter, we report an ultrafast optical spectroscopy study of the response of EuAgAs single crystal after it has been driven out of equilibrium with an ultrashort laser pulse. Our results show that by tuning the magnetic configuration, we can achieve rapid phase transitions between different topological states. This real-time control of topological phases not only complements existing techniques that e.g. rely on external electromagnetic or structural modifications, but also provides a novel method for manipulating quantum states.

\* Corresponding author: peter.oppeneer@physics.uu.se

† Corresponding author: jqmeng@csu.edu.cn

High-quality single crystals of EuAgAs were synthesized using Bi-flux methods, with a  $T_N$  of approximately 12 K [20, 37] (see details in the Supplementary Materials [38]). Ultrafast differential reflectivity  $\Delta R/R$  measurements were carried out at a center wavelength of 800 nm ( $\sim 1.55$  eV) using a Yb-based femtosecond laser oscillator operating at 1 MHz with a pulse width of  $\sim 35$  fs. The pump and probe beams were focused onto the sample in a high vacuum environment ( $< 10^{-6}$  Torr). The spot sizes were  $\sim 140$   $\mu\text{m}$  and  $\sim 60$   $\mu\text{m}$  for the pump and probe, respectively. The pump beam was  $s$ -polarized, and the probe beam was  $p$ -polarized. Further details of the experimental setup are available elsewhere [24].

The sensitivity of ultrafast spectroscopy to near-Fermi-level excitations makes it particularly well-suited for studying topological materials, where the electronic structure plays a crucial role. Figure 1(a) presents typical transient differential reflectivity  $\Delta R/R$  as a function of delay time over a temperature range from 4 to 275 K at a low pump fluence of  $\sim 13$   $\mu\text{J}/\text{cm}^2$ . Photoexcitation creates non-thermal electron and hole distributions that heat the electron gas, resulting in rapid  $\Delta R/R$  changes. Thereafter, a rapid recovery of the change of photoinduced reflectivity occurred within  $\sim 1$  ps. Notably, the  $\Delta R/R$  signal maintains a temperature-independent lineshape across the full range of measurements, but the amplitude of the signal exhibits strong temperature dependence, particularly around  $T_N$ . Below  $T_N$ , EuAgAs enters an AFM phase, and the change in  $\Delta R/R$  amplitude suggests that the AFM ordering significantly modifies the low-energy electronic structure near  $E_F$ .

The 2D pseudocolor map in Fig. 1(b) highlights this temperature dependence more clearly. In particular, around  $T_N$ , there is a noticeable suppression in the  $\Delta R/R$  amplitude, which points to a phase transition driven by the onset of AFM order. This transition is accompanied by a substantial change in the electronic band structure, as the system evolves from a PM Dirac semimetal state to an AFM topological state. Additionally, a local minimum in amplitude is observed in the temperature range of 30 K to 50 K, which closely corresponds to the magnetic fluctuations detected in transport measurements (see details in the Supplementary Materials [38]).

A quantitative analysis of quasiparticle dynamics was performed to examine its temperature-dependent behavior. The solid black lines in Fig. 1(a) indicate that, across all measured temperature ranges, the transient reflectivity over the measured time domain fits well with

$$\frac{R(t)}{R} = \frac{1}{\sqrt{2\pi}w} \exp\left(-\frac{t^2}{2w^2}\right) \otimes \left[ \sum_{i=1}^2 A_i \left(1 - \exp\left(-\frac{t}{\tau_{\text{buildup}}}\right)\right) \exp\left(-\frac{t}{\tau_i}\right) + C \right] \quad (1)$$

where  $A_i$  and  $\tau_i$  represent the amplitude and relaxation time of the  $i$ th decay process,  $\tau_{\text{buildup}}$  is the finite time required to build up the non-equilibrium quasiparticle population,  $w$  is the incident pulse temporal duration, and  $C$  is a constant offset. For the low fluence regime, the transient reflectivity data can be well fitted with a single-exponential decay ( $i = 1$ ).

Figure 1(c) summarizes the temperature dependence of am-

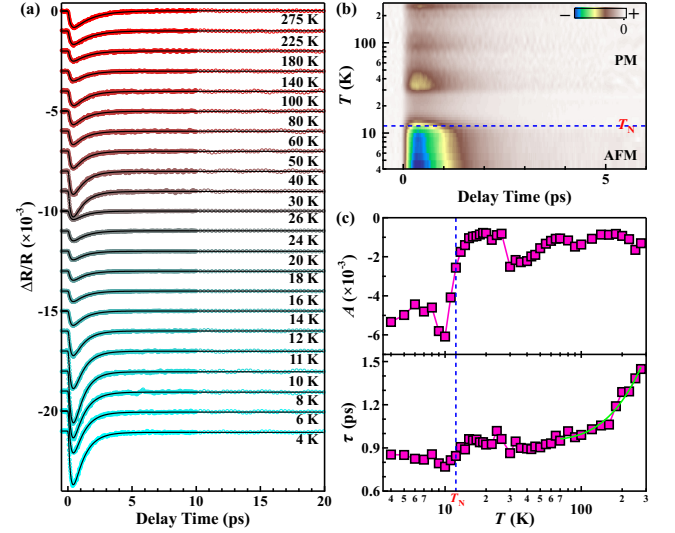


FIG. 1. **Temperature-Dependent Transient Reflectivity in EuAgAs.** (a) Transient differential reflectivity  $\Delta R/R$  as a function of delay time at various temperatures, ranging from 4 K to 275 K, measured at a pump fluence of  $\sim 13$   $\mu\text{J}/\text{cm}^2$ . The black solid lines are fits with Eq. (1). (b) 2D pseudocolor map showing  $\Delta R/R$  as a function of both temperature and delay time. The logarithmic temperature scale highlights significant changes near  $T_N$ , indicating the influence of AFM ordering on the electronic structure. (c) Extracted amplitude  $A$  (upper panel) and relaxation time  $\tau$  (lower panel) as functions of temperature, showing clear anomalies around  $T_N$ . The green solid line represents a TTM fit.

plitude  $A_1$  and relaxation time  $\tau_1$ . The extracted parameters reveal clear anomalies at  $T_N$ , where both the amplitude and relaxation time undergo significant changes. In general, electron-electron scattering rapidly thermalizes the electron and hole distributions within tens of femtoseconds. Subsequently, hot carriers transfer their excess energy to the lattice system through electron-phonon ( $e$ - $ph$ ) scattering, which typically occurs on a picosecond timescale in semimetals [39–44]. At higher temperatures, EuAgAs has been suggested as a non-magnetic topological Dirac semimetal [18]. Similar to other Dirac semimetals [41–44], the ultrafast relaxation dynamics of hot Dirac fermionic quasiparticles in EuAgAs exhibit a comparable timescale ( $\sim 1$  ps), suggesting a dominant  $e$ - $ph$  scattering mechanism. The solid green line in Fig. 1(c) represent a fit using a two-temperature model (TTM) [39, 40], which describes the thermalization process between electrons and the lattice via  $e$ - $ph$  scattering. The excellent fit across large temperature range indicates that  $e$ - $ph$  scattering is the dominant relaxation mechanism in EuAgAs. However, it's important to note that in EuAgAs, electron-hole ( $e$ - $h$ ) recombination can also contribute to the fast decay process, as it doesn't require phonon mediation due to the overlapping conduction and valence bands at the same  $k$  point.

Fluence-dependent measurements of transient reflectivity were employed to explore potential photoinduced phase transitions. Figure 2 shows the fluence-dependent transient reflectivity ( $\Delta R/R$ ) measurements of EuAgAs, highlighting the distinct behavior of the material in both the AFM phase and

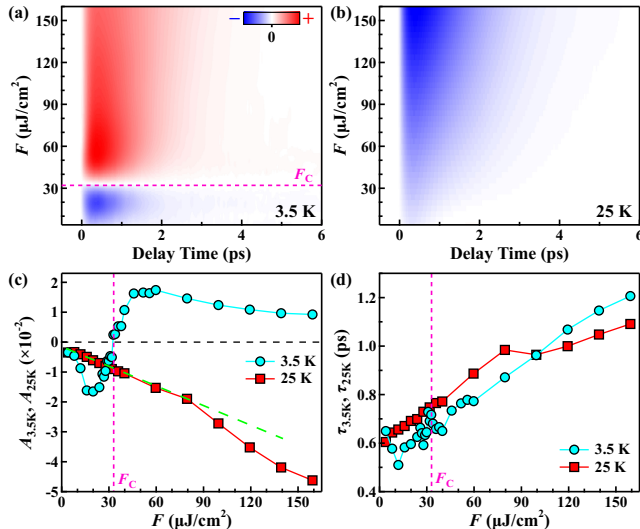


FIG. 2. **Fluence Dependence of Transient Reflectivity.** (a-b) 2D pseudocolor  $\Delta R/R$  maps vs pump-probe delay and temperature (3.5 K, 25 K). (c) and (d) Extracted amplitude  $A$  and relaxation time  $\tau$  of the initial decay, respectively, as functions of pump fluence  $F$ .

the PM phase. These measurements were performed at 3.5 K (below  $T_N$ ) and 25 K (above  $T_N$ ), with the pump fluence varying from low to high, providing insight into how laser fluence influences the material’s magnetic and electronic properties.

In Figure 2(a), the 2D pseudocolor map at 3.5 K shows a striking fluence-dependent change in  $\Delta R/R$ . As the pump fluence increases, a clear transition is observed at a critical fluence ( $F_C \approx 33 \mu\text{J}/\text{cm}^2$ ), where the sign of  $\Delta R/R$  switches from negative to positive. This sign reversal is indicative of a fluence-induced phase transition from an AFM state to a transient FM state. The data reveal that increasing fluence beyond  $F_C$  alters the magnetic configuration, leading to a modification of the electronic structure. This transition is likely accompanied by a topological phase change from a Dirac semimetal state in the AFM phase to a Weyl semimetal state in the transient FM phase. In contrast, Figure 2(b) shows the fluence dependence at 25 K, where the system is in the PM phase. Here, the transient reflectivity decreases monotonically with increasing fluence, and no sign reversal is observed. This suggests that in the PM phase, the system is less responsive to changes in fluence, and a complete PM-to-FM phase transition is not induced within the fluence range explored in this experiment.

To quantitatively analyze quasiparticle relaxation dynamics, we fitted the transient reflectivity data using Eq. (1). For the temperature below  $T_N$ , the transient reflectivity curves fit well a single-exponential decay for all pump fluences (see Fig. S3 in the Supplemental Material [38]). While for the temperature above  $T_N$ , the transient reflectivity curves can be well fitted by Eq. (1) with a single-exponential decay below a pump fluence of  $80 \mu\text{J}/\text{cm}^2$  (see Fig. S4 in the Supplemental Material [38]). However, to achieve a good fit, a second component with positive amplitude should be included (see Fig. S5 in the Supplemental Material [38]). The positive amplitude (both below and above  $T_N$ ) indicates different relaxation

channel that is absent at the low pump fluence.

Figures 2(c) and 2(d) summarize the extracted amplitude  $A$  and relaxation time  $\tau$  of the initial fast decay as functions of pump fluence  $F$ , respectively, for temperatures of 3.5 K and 25 K. At 3.5 K, as shown in Figure 2(c), the amplitude ( $A_{3.5K}$ ) initially decreases with increasing fluence, reaching a minimum around  $15 \mu\text{J}/\text{cm}^2$ . As fluence approaches  $F_C$ , the amplitude crosses zero and becomes positive, indicating the onset of the FM phase. Beyond  $F_C$ , the amplitude increases sharply and saturates between  $\sim 45$  and  $60 \mu\text{J}/\text{cm}^2$ . At 25 K, the amplitude ( $A_{25K}$ ) shows a linear decrease with increasing fluence, without any abrupt transitions, further confirming that the PM state is less sensitive to fluence-driven phase changes. Similarly, Figure 2(d) shows that the relaxation time at 3.5 K ( $\tau_{3.5K}$ ) exhibits anomalies around  $F_C$ , gradually increasing as the fluence rises. This increase in  $\tau_{3.5K}$  suggests that higher fluences lead to slower relaxation dynamics, likely due to the formation of a transient FM phase. In contrast, the relaxation time at 25 K ( $\tau_{25K}$ ) follows a more linear trend, showing a steady increase with fluence, but without the anomalies seen at 3.5 K.

The fluence-dependent behavior of EuAgAs reveals a clear distinction between its response in the AFM and PM phases. In the AFM phase, the material undergoes a laser-induced magnetic phase transition at a critical fluence, which is accompanied by a topological phase transition from a Dirac semimetal to a Weyl semimetal. This transition is not observed in the PM phase, where the electronic structure remains stable under increasing fluence. These results provide strong evidence that EuAgAs is highly tunable via ultrafast optical excitation, making it a promising platform for controlling topological and magnetic phases in real-time.

The question arises: what accounts for the fluence dependence of such a large difference in transient reflectivity between below and above  $T_N$ ? This stark distinction underscores the potential influence of distinct low-energy electron structures, such as magnetic topological mirror semimetal [18] or Dirac semimetal [20] in the AFM phase and Dirac semimetal in the PM phase [18], on carrier dynamics following laser excitation in EuAgAs. We consider three possible mechanisms to explain this fluence-dependent disparity: (i) Laser-induced thermal effects. One explanation could be that intense laser pulses result in substantial heating of the sample surface, causing the local temperature to rise and potentially inducing a phase transition from AFM to PM near the surface. While this scenario might explain a gradual transition, it is unlikely to account for the sharp fluence threshold and the abrupt sign reversal in reflectivity observed below  $T_N$ . Furthermore, the uniform negative  $\Delta R/R$  response at lower fluences [Fig. 1], regardless of whether the sample is in the AFM or PM phase, suggests that simple thermal effects alone do not explain the fluence-dependent behavior. (ii) Phase-space [44] or band filling [45] effects. Another possible mechanism is phase-space filling or band filling, where high fluence excitation leads to saturation of available electronic states near the Dirac node, limiting further optical absorption due to Pauli blocking. This would result in a positive  $\Delta R/R$  response. However, such effects should occur similarly in both the AFM and PM phases,

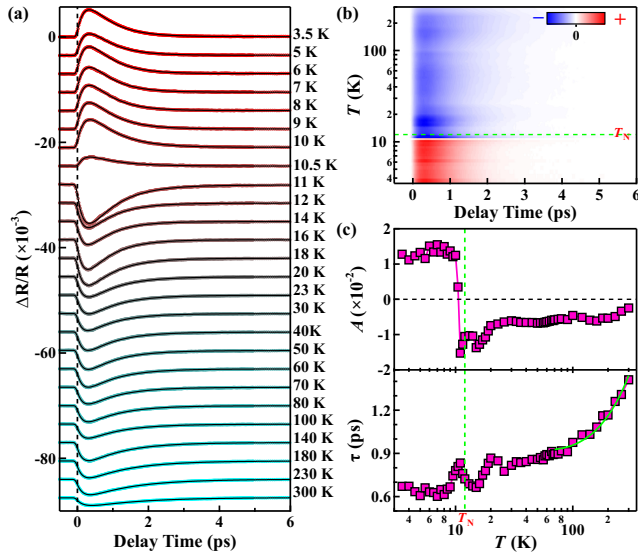


FIG. 3. **Evolution of Ultrafast Reflectivity with Temperature in EuAgAs.** (a)  $\Delta R/R$  as a function of delay time over a wide temperature range from 3.5 to 300 K, measured at a higher pump fluence ( $\sim 60 \mu\text{J}/\text{cm}^2$ ). The black solid lines are fits with Eq. (1). (b) 2D pseudocolor map of  $\Delta R/R$  as a function of temperature and delay time. (c) Extracted amplitude  $A$  (upper panel) and relaxation time  $\tau$  (lower panel) as a function of temperature. The solid green line shows the TTM fit.

as they do not depend on the magnetic ordering. The lack of a similar response above  $T_N$  suggests that phase-space filling is not the primary cause of the fluence-dependent behavior below  $T_N$ . (iii) photoinduced topological phase transition [22, 31, 32]. The most likely explanation for the observed fluence dependence is a photoinduced topological phase transition that is closely tied to the material's magnetic order. Femtosecond laser pulses can effectively regulate the magnetic state [46, 47]. The laser can induce a direct deflection of the magnetic moment. Below  $T_N$ , EuAgAs is highly susceptible to external perturbations due to its metamagnetic nature. Femtosecond laser pulses can induce a rapid transition from the AFM state to a transient FM state, accompanied by a topological phase transition from a Dirac semimetal to a Weyl semimetal [18, 20]. This transition manifests as a fluence-dependent sign reversal in  $\Delta R/R$ , with the critical fluence ( $F_C$ ) marking the onset of the FM phase. Above  $T_N$ , the system is already in the PM state, and while high fluence may perturb the electronic structure, it does not induce a full transition to the FM state, resulting in a monotonic decrease in reflectivity without a sign reversal.

To further test our hypothesis, a detailed temperature-dependent measurement was carried out with a higher fluence of  $\sim 60 \mu\text{J}/\text{cm}^2$ . Figure 3(a) displays transient reflectivity  $\Delta R/R$  at selected temperatures, while Fig. 3(b) presents a 2D pseudocolor map of  $\Delta R/R$  as a function of pump-probe delay time and temperature. At low temperatures, the radiation region is already in the photoinduced transient FM phase. As the temperature increases, the transient reflectivity  $\Delta R/R$  shifts from positive to negative at approximately 10.5 K, which is slightly below  $T_N$ . It can be found that the relaxation process

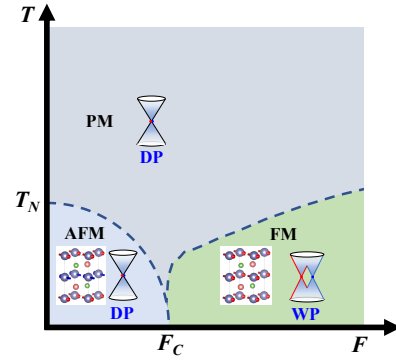


FIG. 4. **Light-Induced Topological Phase Transitions via Magnetic Order Tuning in EuAgAs.** Schematic phase diagram illustrating the light-induced topological phase transition in EuAgAs. In the AFM phase (below  $T_N$ ), a pair of Dirac points transitions to Weyl points upon increasing pump fluence beyond  $F_C$ , corresponding to a magnetic transition from AFM to a transient FM state. In the PM phase (above  $T_N$ ), Dirac points persist but are less responsive to fluence, as indicated by the lack of a complete PM-to-FM transition. The arrows represent the magnetic moments of Eu ions, and the dashed lines are guides to the eye, illustrating the fluence- and temperature-dependent behavior of the topological phase transitions.

at higher temperatures shows similarities to that observed at low fluence [Fig. 1(a)]: within the magnetic fluctuation temperature region, complex temperature-dependent behavior occurs, like the wave-shape of  $A_1(T)$  and  $\tau_1(T)$ , and the high-temperature PM phase resembles the  $e$ - $ph$  scattering relaxation process described by the TTM [solid green line in Fig. 3(c)]. It means that, at temperatures above  $\sim 10.5$  K, EuAgAs is dominated by the paramagnetic state. This also actually means that the FM state is difficult to be induced from the PM state by the laser, which is consistent with the conclusion of the fluence-dependent measurement results at 25 K. The high-fluence temperature-dependent experiment further substantiates the intimate correlation between the photoinduced phase transition and the AFM order.

As shown in Fig. 4, we propose a fluence-temperature phase diagram for EuAgAs that provides a simplified representation of its topological and magnetic transitions. In the AFM phase, a pair of Dirac cones exists at low pump fluences. Increasing the laser fluence triggers spin-flip transitions, leading to magnetization and ultimately driving a phase transition to a FM Weyl semimetal state when beyond a critical threshold ( $F_C$ ). In the PM phase, a similar pair of Dirac cones appears at low fluences. While increasing the fluence can indeed induce magnetization in this phase, our experimental observations have not revealed a complete PM-to-FM phase transition within the studied fluence range. This suggests that additional factors, such as temperature or external magnetic fields, may play crucial roles in determining the precise conditions for such a transition.

In this study, we have experimentally demonstrated the occurrence of subpicosecond topological phase transitions in the antiferromagnetic Dirac semimetal EuAgAs through ultrafast laser-induced control of magnetic order. Our experiments reveal a strong coupling between magnetic configuration and

electronic structure, evidenced by the observed shifts in spectral features under varying conditions. Notably, the time-resolved data indicate a rapid response of the system to optical excitation, suggesting that light can effectively induce transitions between topological states. These findings not only enhance our understanding of the interplay between topology and magnetism in EuAgAs but also highlight its potential for applications in quantum technologies. Future work will focus on further elucidating the mechanisms underlying these transitions and exploring their implications for the design of topological materials.

This work was supported by National Key Research and Development Program of China (Grant No. 2022YFA1604204), the National Natural Science Foundation of China (Grant No. 12074436), the Science and Technology Innovation Program of Hunan province (Grant No. 2022RC3068), and Fundamental Research Funds for the Central Universities of Central South University (No. 1053320215412). We further acknowledge support from the K. and A. Wallenberg Foundation (Grants No. 2022.0079 and 2023.0336). This work is carried out in part using computing resources at the High Performance Computing Center of Central South University.

- 
- [1] C. Chang, J. Zhang, X. Feng, J. Shen, Z. Zhang, M. Guo, K. Li, Y. Ou, P. Wei, L. Wang, Z. Ji, Y. Feng, S. Ji, X. Chen, J. F. Jia, X. Dai, Z. Fang, S. C. Zhang, K. He, Y. Y. Wang, L. Lu, X. C. Ma, and Q. K. Xue, *Science* **340**, 167, 1 (2013).
- [2] K. He, Y. Y. Wang, and Q. K. Xue, *Annu. Rev. Condens. Ma. P.* **9**, 329, 1 (2018).
- [3] C. Yue, Y. Xu, Z. Song, H. Weng, Y. Lu, C. Fang, and X. Dai, *Nat. Phys.* **15**, 577 (2019).
- [4] M. Mogi, M. Kawamura, R. Yoshimi, A. Tsukazaki, Y. Kozuka, N. Shirakawa, K. S. Takahashi, M. Kawasaki, and Y. Tokura, *Nat. Mater.* **16**, 516 (2017).
- [5] P. Puphal, V. Pomjakushin, N. Kanazawa, V. Ukleev, D. J. Gawryluk, J. Ma, M. Naamneh, N. C. Plumb, L. Keller, R. Cubitt, E. Pomjakushina, and J. S. White, *Phys. Rev. Lett.* **124**, 017202 (2020).
- [6] S. Roychowdhury, M. Yao, K. Samanta, S. Bae, D. Chen, S. Ju, A. Raghavan, N. Kumar, P. Constantinou, S.N. Guin, N.C. Plumb, M. Romanelli, H. Borrmann, M.G. Vergniory, V.N. Strocov, V. Madhavan, C. Shekhar, and C. Felser, *Adv. Sci.* **10**, 2207121 (2023).
- [7] C. Y. Guo, F. Wu, Z. Z. Wu, M. Smidman, C. Cao, A. Bostwick, C. Jozwiak, E. Rotenberg, Y. Liu, F. Steglich, and H. Q. Yuan, *Nat. Commun.* **9**, 4622 (2018).
- [8] G. Hua, S. Nie, Z. Song, R. Yu, G. Xu, and K. Yao, *Phys. Rev. B* **98**, 201116 (2018).
- [9] S. Xu, Z. Chen, X. Chen, Y. Zhao, H. Xu, and X. Zhang, *Phys. Rev. B* **102**, 125123 (2020).
- [10] J. Soh, S. M. Tobin, H. Su, I. Zivkovic, B. Ouladdiaf, A. Stunault, J. A. Rodríguez-Velamazán, K. Beauvois, Y. F. Guo, and A. T. Boothroyd, *Phys. Rev. B* **104**, L161103 (2021).
- [11] Z. Zhu, G. W. Winkler, Q. Wu, J. Li, and A. A. Soluyanov, *Phys. Rev. X* **6**, 031003 (2016).
- [12] B. Q. Lv, Z. Feng, Q. Xu, X. Gao, J.-Z. Ma, L.-Y. Kong, P. Richard, Y.-B. Huang, V. N. Strocov, C. Fang, H.-M. Weng, Y.-G. Shi, T. Qian, and H. Ding, *Nature (London)* **546**, 627 (2017).
- [13] C. Chen, H. Wang, Z. Yang, and H. Zhang, *Chin. Phys. Lett.* **38**, 057302 (2021).
- [14] Y. Xu, Z. Song, Z. Wang, H. Weng, and X. Dai, *Phys. Rev. Lett.* **122**, 256402 (2019).
- [15] S. X. M. Riberolles, T. V. Trevisan, B. Kuthanazhi, T. W. Heitmann, F. Ye, D. C. Johnston, S. L. Bud Ko, D. H. Ryan, P. C. Canfield, A. Kreyssig, A. Vishwanath, R. J. McQueeney, L. L. Wang, P. P. Orth, and B. G. Ueland, *Nat. Commun.* **12**, 999 (2021).
- [16] J. Ma, H. Wang, S. Nie, C. Yi, Y. Xu, H. Li, J. Jandke, W. Wulfhekel, Y. Huang, D. West, P. Richard, A. Chikina, V. N. Strocov, J. Mesot, H. Weng, S. Zhang, Y. Shi, T. Qian, M. Shi, and H. Ding, *Adv. Mater.* **32**, 1907565 (2020).
- [17] A. Valadkhani, M. Iraola, A. Fünfhaus, Y. Song, L. Šmejkal, J. Sinova, and R. Valentí, *Phys. Rev. B* **108**, 235113 (2023).
- [18] Y. Jin, X. Zeng, X. Feng, X. Du, W. Wu, X. Sheng, Z. Yu, Z. Zhu, and S. A. Yang, *Phys. Rev. B* **104**, 165424 (2021).
- [19] Z. Zhang, X. Chen, C. An, S. Wang, L. Zhang, Y. Zhou, M. Zhang, J. Zhou, and Z. Yang, *Materials Today Physics* **38**, 101228 (2023).
- [20] A. Laha, R. Singha, S. Mardanya, B. Singh, A. Agarwal, P. Mandal, and Z. Hossain, *Phys. Rev. B* **103**, L241112, 1 (2021).
- [21] C. Tomuschat, and H. U. Schuster, *Z. Anorg. Allg. Chem.* **518**, 161-167 (1984).
- [22] T. Dong, S. J. Zhang, and N. L. Wang, *Adv. Mater.* **35**, e2110068 (2023).
- [23] C. Bao, P. Tang, D. Sun, S. Zhou, *Nature Reviews Physics* **4**, 33 (2022).
- [24] C. Zhang, Q. Y. Wu, W. S. Hong, H. Liu, S. X. Zhu, J. J. Song, Y. Z. Zhao, F. Y. Wu, Z. T. Liu, S. Y. Liu, Y. H. Yuan, H. Huang, J. He, S. L. Li, H. Y. Liu, Y. X. Duan, H. Q. Luo, and J. Q. Meng, *Sci. China Phys. Mech. Astron.* **65**, 237411 (2022).
- [25] Y. C. Tian, W. H. Zhang, F. S. Li, Y. L. Wu, Q. Wu, F. Sun, G. Y. Zhou, L. Wang, X. Ma, Q. Xue, J. Zhao, *Phys. Rev. Lett.* **116**, 107001 (2016).
- [26] Q. Y. Wu, C. Zhang, Z. Z. Li, W. S. Hong, H. Liu, J. J. Song, Y. Z. Zhao, Y. H. Yuan, B. Chen, X. Q. Ye, S. L. Li, J. He, H. Y. Liu, Y. X. Duan, H. Q. Luo, J. Q. Meng, *Phys. Rev. B* **108**, 205136 (2023).
- [27] Y. P. Liu, Y. J. Zhang, J. J. Dong, H. Lee, Z. X. Wei, W. L. Zhang, C. Y. Chen, H. Q. Yuan, Y. F. Yang, and J. Qi, *Phys. Rev. Lett.* **124**, 057404 (2020).
- [28] Y. Z. Zhao, Q. Y. Wu, C. Zhang, B. Chen, W. Xia, J. J. Song, Y. H. Yuan, H. Liu, F. Y. Wu, X. Q. Ye, H. Y. Zhang, H. Huang, H. Y. Liu, Y. X. Duan, Y. F. Guo, J. He, J. Q. Meng, *Phys. Rev. B* **108**, 075115 (2023).
- [29] V. Iyer, Y. P. Chen, and X. Xu, *Phys. Rev. Lett.* **121**, 026807 (2018).
- [30] H. Liu, Q. Y. Wu, C. Zhang, J. Pang, B. Chen, J. J. Song, Y. X. Duan, Y. H. Yuan, H. Y. Liu, C. C. Shu, Y. F. Xu, Y. G. Shi, and J. Q. Meng, *Phys. Rev. B* **110**, 195104 (2024).
- [31] L. Luo, D. Cheng, B. Song, L. Wang, C. Vaswani, P. M. Lozano, G. Gu, C. Huang, R. H. J. Kim, Z. Liu, J. Park, Y. Yao, K. Ho, I. E. Perakis, Q. Li, J. Wang, *Nature Materials* **20**, 329-334 (2021).
- [32] E. J. Sie, C. M. Nyby, C. D. Pemmaraju, S. J. Park, X. Shen, J. Yang, M. C. Hoffmann, B. K. Ofori-Okai, R. Li, A. H. Reid, S.

- Weathersby, E. Mannebach, N. Finney, D. Rhodes, D. Chenet, A. Antony, L. Balicas, J. Hone, T. P. Devereaux, T. F. Heinz, X. Wang, and A. M. Lindenberg, *Nature* **565**, 61 (2019).
- [33] Y. H. Wang, H. Steinberg, P. Jarillo-Herrero, and N. Gedik, *Science* **342**, 453 (2013).
- [34] M. S. Rudner, and N. H. Lindner, *Nat. Rev. Phys.* **2**, 229 (2020)
- [35] S. H. Zhou, C. H. Bao, B. S. Fan, H. Zhou, Q. X. Gao, H. Y. Zhong, T. Y. Lin, H. Liu, P. Yu, P. Z. Tang, S. Meng, W. H. Duan, and S. Y. Zhou, *Nature* **614**, 75 (2023).
- [36] M. Y. Zhang, Z. X. Wang, Y. N. Li, L. Y. Shi, D. Wu, T. Lin, S. J. Zhang, Y. Q. Liu, Q. M. Liu, J. Wang, T. Dong, and N. L. Wang, *Phys. Rev. X* **9**, 021036 (2019).
- [37] J. Tong, J. Parry, Q. Tao, G. Cao, Z. Xu, and H. Zeng, *J. Alloy. Compd.* **602**, 26 (2014).
- [38] See Supplemental Material for details on single crystal synthesis, transport characterization, and additional transient reflectivity data.
- [39] S. X. Zhu, C. Zhang, Q. Y. Wu, X. F. Tang, H. Liu, Z. T. Liu, Y. Luo, J. J. Song, F. Y. Wu, Y. Z. Zhao, S. Y. Liu, T. Le, X. Lu, H. Ma, K. H. Liu, Y. H. Yuan, H. Huang, J. He, H. Y. Liu, Y. X. Duan, and J. Q. Meng, *Phys. Rev. B* **103**, 115108 (2021).
- [40] L. Cheng, F. C. Fei, H. Hu, Y. M. Dai, F. Q. Song, J. Qi, *Phys. Rev. B* **106**, 104308 (2022).
- [41] D. Sun, Z. Wu, C. Divin, X. Li, C. Berger, W. A. de Heer, P. N. First, and T. B. Norris, *Phys. Rev. Lett.* **101**, 157402 (2008).
- [42] P. A. George, J. Strait, J. Dawlaty, S. Shivaraman, M. Chandrashekar, F. Rana, and M. G. Spencer, *Nano Lett.* **8**, 4248 (2008).
- [43] W. Lu, S. Ge, X. Liu, H. Lu, C. Li, J. Lai, C. Zhao, Z. Liao, S. Jia, and D. Sun, *Phys. Rev. B* **95**, 024303 (2017).
- [44] C. P. Weber, *J. Appl. Phys.* **129**, 070901 (2021).
- [45] G. Zhai, C. Ma, J. Xiang, J. Ye, T. Li, Y. Li, P. Sun, G. Chen, X. Wu, and X. Zhang, *Phys. Rev. B* **101**, 174310 (2020).
- [46] I. Žutić, J. Fabian, and S. Das Sarma, *Rev. Mod. Phys.* **76**, 323 (2004).
- [47] A. Hirohata, K. Yamada, Y. Nakatani, I. Prejbeanu, B. Diény, P. Pirro, and B. Hillebrands, *Journal of Magnetism and Magnetic Materials* **509**, 166711 (2020).